THE ASTROPHYSICAL JOURNAL, 418:894–898, 1993 December 1

CYGNUS X-3 IN AN "ULTRAHIGH" X-RAY STATE WITH NO DETECTED Kα LINE EMISSION

A. P. SMALE,[1] R. F. MUSHOTZKY,[2] E. M. SCHLEGEL,[1] K. A. WEAVER,[2,3] P. J. SERLEMITSOS,[2]
F. E. MARSHALL,[2] R. PETRE,[2] AND K. JAHODA[2]
Laboratory for High-Energy Astrophysics, NASA/Goddard Space Flight Center, Greenbelt, MD 20771
Received 1993 February 24; accepted 1993 June 8

ABSTRACT

Cyg X-3 is well-known to be the brightest source of 6.7 keV iron K-line photons in the X-ray sky; this line has been unambiguously detected in data from *OSO 8*, *Ariel 5*, *HEAO 1* A-2, the *EXOSAT* GSPC, *Tenma*, and *Ginga*, with measured physical widths (FWHM) ranging from 0.6 to 1.0 keV and equivalent widths typically from 0.5 to 1.7 keV. However, when the Shuttle-borne X-ray telescope BBXRT observed this source on 1990 December 5, the line was not detected.

The BBXRT data show Cyg X-3 to be in an unusually high, soft state, with a luminosity of $\sim 2 \times 10^{38}$ ergs s^{-1} (1–10 keV; at 10 kpc), above the Eddington limit. The continuum is well described by a blackbody with temperature $kT = 1.13 \pm 0.02$ keV, constituting 93% of the flux, plus an additional soft component. No iron line is seen in the spectrum, with formal 99% confidence upper limits on the equivalent width of 160 eV, 120 eV, and 75 eV for lines with FWHM = 1 keV, 600 eV, and 200 eV, respectively, for a line in the energy range 6.1–7.1 keV. Ninety percent confidence limits are typically 20 eV lower.

We discuss these results in the context of the various physical models for Cyg X-3, and conclude that the high X-ray luminosity can be attributed to an increase in the blackbody component from the neutron star surface and inner accretion disk. We speculate that an increase in the mass-accretion rate may have caused the inner disk to become optically and geometrically thick, shielding the outer disk and much of the corona from the bulk of the central X-ray flux. Alternatively, a decrease in the extent of the azimuthal structure on the disk edge may have resulted in greater visibility of the central X-ray emitting region.

Subject headings: binaries: close — stars: individual (Cygnus X-3) — X-rays: stars

1. INTRODUCTION

Cyg X-3 is simultaneously one of the best-studied and most enigmatic X-ray sources in the Galaxy. Its X-ray flux is modulated on a 4.79 hr period, indicating that it is a close binary system, and this period is increasing with a derivative of $\sim 10^{-9}$ s s^{-1}, and a possible $\ddot{P}$ term (van der Klis & Bonnet-Bidaud 1989). It has high and low X-ray states which may be due to changes in the mass-accretion rate or the structure of an accretion disk. Long-term X-ray observations with *Vela 5B* show that Cyg X-3 switches between these states every 0.5–2 yr, showing considerable luminosity variations within each, and displays a shot-noise–type variation with a characteristic timescale of ~100 days (Priedhorsky & Terrell 1986; Smale & Lochner 1992). Oscillations with periods ranging from 50 s to 1500 s have also been observed (van der Klis & Jansen 1985).

Several different models have been put forward for the X-ray emission from Cyg X-3. In the first model, the X-ray emission is powered by accretion through a disk via Roche lobe overflow. A corona of material is evaporated off the disk surface by the irradiating compact object, and the variable obscuration of this corona by material at the disk edge produces the 4.8 hr modulation (White & Holt 1982). In the second, no accretion disk is present and the compact object orbits within an optically thick scattering cloud centered upon the companion (Pringle 1974; Davidsen & Ostriker 1974). The third model has the Cyg X-3 system enclosed by a large shell or cocoon (Milgrom 1976; Bonnet-Bidaud & van der Klis 1981).

In the radio, Cyg X-3 displays extremely large outbursts, reaching $S_\nu > 21$ Jy at 10 GHz (Gregory et al. 1972), during which a double-sided relativistic jet can be detected along a roughly north–south axis (Spencer et al. 1986; Molnar, Reid, & Grindlay 1988). Coordinated X-ray and infrared flares have been observed (Mason, Córdova, & White 1986). The possible detection of a fast 10^{12} eV pulsar with period 12.59 ms (Chadwick et al. 1985) is not confirmed at X-ray energies (Kitamoto et al. 1992). Finally, strong He I and He II emission is observed in the infrared (van Kerkwijk et al. 1992), indicating the existence of a strong wind which may originate in a Wolf-Rayet companion.

Most importantly for this paper, Cyg X-3 is known to be the brightest source of 6.7 keV iron Kα-line photons in the X-ray sky; this line has been unambiguously detected by every orbiting X-ray experiment with the capability of studying it from *OSO 8* to *Ginga*. We present here the results of a BBXRT observation which show the source in an unusually high state with a rarely seen continuum shape and no detectable iron line emission, and discuss possible physical causes for these findings.

2. THE BBXRT OBSERVATIONS

The Broad-Band X-Ray Telescope (BBXRT) flew on the Space Shuttle Columbia on 1990 December 2–December 11, as part of the Astro 1 payload. The flight of BBXRT marked the first opportunity for performing X-ray observations over a broad energy range (0.3–12 keV) with a moderate energy resolution (typically 90 eV and 150 eV at 1 and 6 keV,

[1] Code 668; also Research Scientist, Universities Space Research Association.
[2] Code 666, NASA/GSFC.
[3] Also University of Maryland.

respectively). This energy resolution, coupled with an extremely low detector background of 1.2×10^{-3} counts keV^{-1} s^{-1}, makes BBXRT a powerful tool for the study of continuum and line emission from X-ray binaries and other cosmic sources.

The BBXRT instrument (Serlemitsos et al. 1992) consists of two co-aligned telescopes of 3.8 m focal length, each containing a thin-foil conical mirror assembly and a segmented, cryogenically cooled Si(Li) detector. Each detector is subdivided into five pixels, each with 512 energy channels. The central pixels (A0, B0) have a field-of-view 4′ in diameter, and the outer pixels (A1–A4, B1–B4) extend the total field of view to 17′.4. The B detector is rotated by 180° relative to the A detector such that, e.g., A1 and B3 co-observe the same area on the sky. The pixels are separated by a mask 1′.5 across.

Cyg X-3 was observed on 1990 December 5th, 00:21:04 UT, for 400 s. After the Crab and Cyg X-2, Cyg X-3 was the brightest source observed by BBXRT, with a count rate over all pixels of 238 counts s^{-1}. The time of observation corresponds to phase $\phi = 0.18$ according to the parabolic ephemeris of van der Klis & Bonnet-Bidaud (1989), and $\phi = 0.30$ according to their cubic ephemeris. Cyg X-3 was observed 2′.6 off-axis, such that the flux from the source fell mainly into the A2 and A1 (B4 and B3) pixels. Figure 1 shows the fields of view of the BBXRT pixels projected onto an X-ray map of the Cyg X-3 region derived from an *Einstein* IPC image. The Cyg OB2 association (Harnden et al. 1979) is visible at the top of the IPC field, half a degree from Cyg X-3 and therefore well out of the BBXRT field of view.

3. RESULTS

In Figure 2 we show the raw BBXRT data observed in the B4 pixel. There is no evidence for the broad, intense iron emission between 6 and 8 keV observed by previous satellites. To demonstrate this, we constructed two simulated data sets by folding the best-fitting continuum through the BBXRT spectral response with the same counting statistics as the real data and adding an iron line with the parameters derived in previous observations. The figure shows that, had the line emission been at previously determined levels, it would have been clearly visible in the raw data.

We performed continuum fits on the spectra from pixels A1, A2, B3, and B4 individually, and found no significant differences in the spectral parameters derived in each case. The signal-to-noise ratio can be improved by fitting several pixels simultaneously, forcing physical parameters such as photon index and temperatures to be common for each pixel but allowing the individual pixel normalizations to vary. In this way we performed a simultaneous fit to the data from these four pixels, with a total source counting rate of 195 counts s^{-1}, background making up less than 0.2% of this rate. The best fit (Fig. 3) was found to be a blackbody of temperature $kT_1 = 1.136 \pm 0.015$ keV, plus a soft component that could be represented equally well by a power law with energy index $\alpha = 4.3 \pm 0.3$, a second blackbody with $kT_2 = 0.26 \pm 0.01$ keV, or a thermal bremsstrahlung with temperature $kT_3 = 0.47 \pm 0.04$ keV. In each case the final χ^2 was ~ 1500 for 1370 degrees of freedom, and the second component contributed

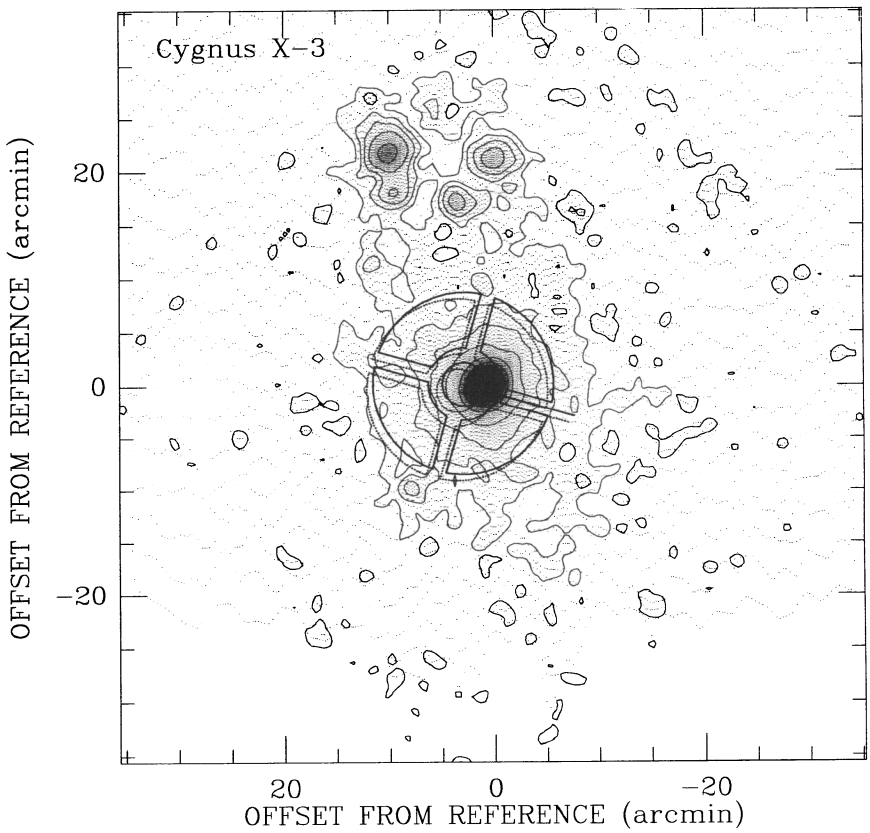

FIG. 1.—BBXRT pixel configurations projected onto a contour plot showing the X-ray surface brightness distribution of the Cyg X-3 region, derived from an *Einstein* IPC image (sequence no. 3378, obtained on 1978 day 350, 5192 s). The image is centered at R.A. = $20^h30^m32^s.6$, Decl. = +40°47′06″ (1950.0), and north is at the top of the figure. The contour levels represent 0.2, 0.5, 1, 2, 5, 10, 20 and 50% of the peak flux in the image. Cyg X-3 dominates the flux at the center of the field, while stellar sources Cyg OB2 nos. 8, 5, 12, and 9 are visible at the top. The diffuse X-ray emission from the OB association is ~2 orders of magnitude fainter than Cyg X-3. The solid line shows the field of view and orientation of the pixels in the A-detector; the dotted line, the B pixels. The A1/A2 (B3/B4) border is also marked.

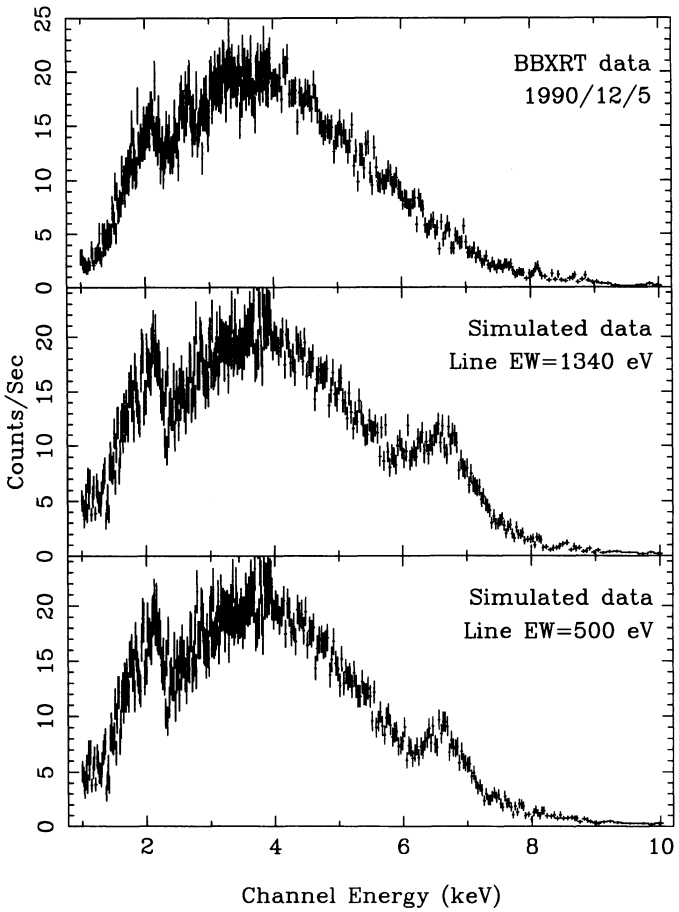

FIG. 2.—(*a*) The raw BBXRT data observed in B4 on 1990 December 5. No iron line is visible in the raw data. (*b*) A simulated spectrum with the same continuum parameters and counting statistics as the real data, plus a line at $E = 6.76$ keV with equivalent width EW = 1340 eV and FWHM = 1.0 keV, as observed by *HEAO 1* (White & Holt 1982). (*c*) A spectrum simulated as before, but with line parameters $E = 6.70$ keV, FWHM = 600 eV, EW = 500 eV, as observed with the *EXOSAT* GSPC (van der Klis et al. 1985). The feature at 2.2 keV is the gold M edge from the mirrors.

only 7% of the 1–10 keV flux. The derived column density N_H was $(4.89 \pm 0.50) \times 10^{22}$ atoms cm^{-2}, and a contour plot of N_H against blackbody temperature kT_1 is shown in Figure 4. The combined spectra from the central pixels A0 and B0 give similar spectral fit parameters for each component but with a much reduced accuracy due to the lower counting rate. We attempted to include an explicit term in the fit to model the known X-ray halo of Cyg X-3 (Mauche & Gorenstein 1986; Molnar & Mauche 1986) but found that the halo parameters played off against the hydrogen column density, leading to convergence problems.

Attempts to improve the fit by adding a line between 6 and 7 keV were not encouraging. Fits with all parameters free quickly produced "lines" with very small equivalent widths, energies tending toward 6 keV, and nonsensically broad physical widths. Fixing the line energy and/or width, we obtained a reduction in χ^2 of less than 10, insufficient to be statistically significant.

We thus proceeded to determine the formal upper limit on the Fe-line emission for a range of physical line widths. Values of the line energy were stepped from 6.1 to 7.1 keV in steps of 0.1 keV, while the relative normalizations of the Gaussian component for each of the four pixels were stepped at their corresponding continuum ratios until χ^2 increased by 6.63, representing 99% confidence for one parameter of interest. The equivalent width was then computed. In this way, we obtained firm upper limits on the line equivalent width of 160 eV, 120 eV, 110 eV, and 75 eV, respectively, for lines with physical widths of 1 keV, 600 eV, 400 eV, and 200 eV. (The 90% confidence limits are typically ~20 eV lower.) These results are displayed in Figure 5.

The literature on Cyg X-3 from *Uhuru* to *Ginga*, including long-term monitoring programs by *Vela 5B* and *Ariel* 5 (Smale & Lochner 1992; Holt et al. 1979), shows that the source usually lies in the intensity range 2×10^{37}–1.2×10^{38} ergs s^{-1} (at 10 kpc). After correcting for flux vignetting by the mask, the total 1–10 keV luminosity measured during our BBXRT observation was 2.1×10^{38} ergs s^{-1}. Thus, we observed Cyg X-3 in an unusually bright state, above the Eddington limit provided that the mass of the compact object is less than 1.75 $M_\odot$ and the hydrogen mass fraction exceeds 0.14.

The apparent faintness of the iron line is not, however, merely an artifact of the increased continuum emission. If line emission is still present it must be at a very low *absolute* level. For a line with a physical width of 200–600 eV, the 99% upper limits on the equivalent width translate to a line intensity of 0.003–0.007 photons cm^{-2} s^{-1}, considerably smaller than the previously measured lower bounds on line emission from the source (by *Tenma*; Kitamoto et al. 1987).

4. DISCUSSION

From the major body of literature that exists on Cyg X-3, a unified picture of its X-ray spectral behavior is beginning to emerge. In its high state, the spectrum consists of the following:

1. A power-law component with a high-energy cutoff (or Comptonization spectrum), with typical photon index ~2–3 (e.g., Blissett, Mason, & Culhane 1977; White & Holt 1982; Kitamoto et al. 1987; Nakamura et al. 1993);
2. A blackbody with a temperature of $kT \sim 1.1$ keV and blackbody radius $R_{bb} \sim 10$ km, sometimes with its own additional absorption term (Nakamura et al. 1993);
3. A broad iron line, with energy measured variously as 6.5 keV (e.g., Kestenbaum et al. 1978; Blissett et al. 1981; Nakamura et al. 1993), 6.7 keV (e.g., White & Holt 1982; van der Klis et al. 1985; Kitamoto et al. 1987), and 6.95 keV (Rajeev et al. 1993). Line parameters for all observations up to and including *Tenma* are conveniently summarized in Kitamoto et al. (1987; Table 7), with the FWHM typically 0.6–1.0 keV and the equivalent widths ranging from 0.5 to 1.7 keV;
4. An iron edge at ~9 keV (Kitamoto et al. 1987; Nakamura et al. 1993) and a possible edge at 7.1 keV from neutral iron (Rajeev et al. 1993).

The low-state spectrum has similar continuum components, but with differing intensities and best-fit parameters; $\alpha \sim 1.0$–1.3 (e.g., Becker et al. 1978); $kT_{bb} \sim 1.0$ keV, $R_{bb} \sim 8$ km (Nakamura et al. 1993); $kT_{bb} \sim 2.4$ keV, $R_{bb} \sim 2.5$ km (Rajeev et al. 1993). The blackbody contribution is greatly reduced in the low state. Some workers find that the energy and width of the iron line are similar in the two states (e.g., Nakamura et al. 1993), while others find significantly lower line energies and widths in the low state (Rajeev et al. 1993).

The BBXRT observation of Cyg X-3 does not fit neatly into this general picture. First, it is clear we caught the source in an unprecedented "ultrahigh" state relative to previous flux measurements. This can be parameterized as a 10-fold increase in

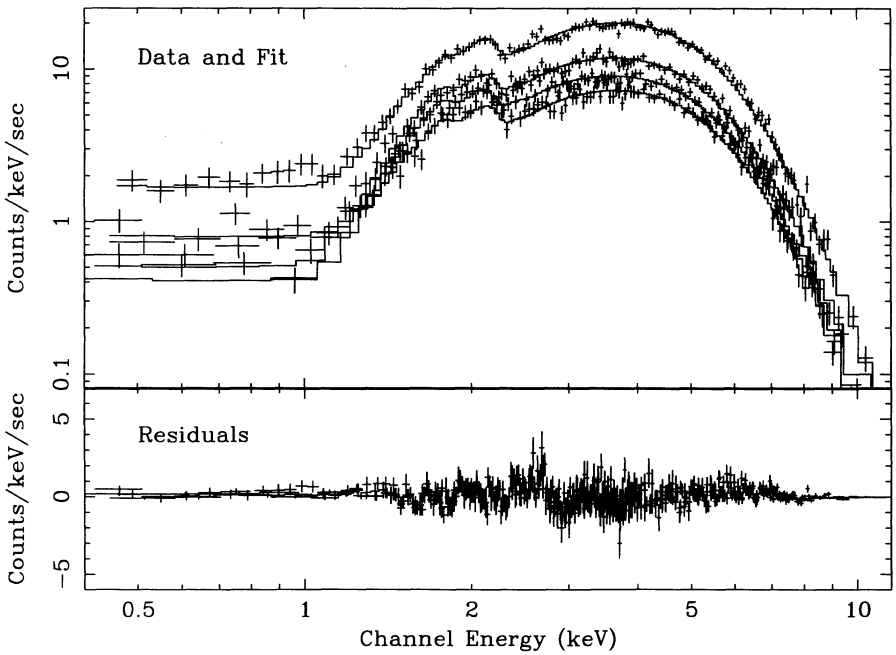

FIG. 3.—The spectrum and best fit to the BBXRT data. A simultaneous fit was performed to four BBXRT pixels; in order of decreasing count rate these are B4, A2, A1, and B3. The best-fit model is a blackbody spectrum with $kT = 1.13$ keV and $N_H = 4.9 \times 10^{22}$ cm^{-2}, plus a 7% contribution from a soft component (see text). The spectra have been rebinned for presentational purposes.

the intensity of the blackbody component over that measured in the normal "high" state. Also, we find only upper limits on iron line emission.

Physical interpretations of the spectral behavior and the modulation of the light curve with orbital phase and energy fall into three main classes, each involving the scattering of X-rays into the line of sight. In the accretion disk corona (ADC) model (White & Holt 1982), the X-rays are scattered by the ADC and modulated by structure on the accretion disk rim. An alternate model has the X-rays scattered by a stellar wind centered on the companion star, and modulated by optical depth effects (Pringle 1974; Davidsen & Ostriker 1974). In a third model the X-ray photons are scattered by a large shell enclosing the binary and modulated by the shadowing of this shell by the

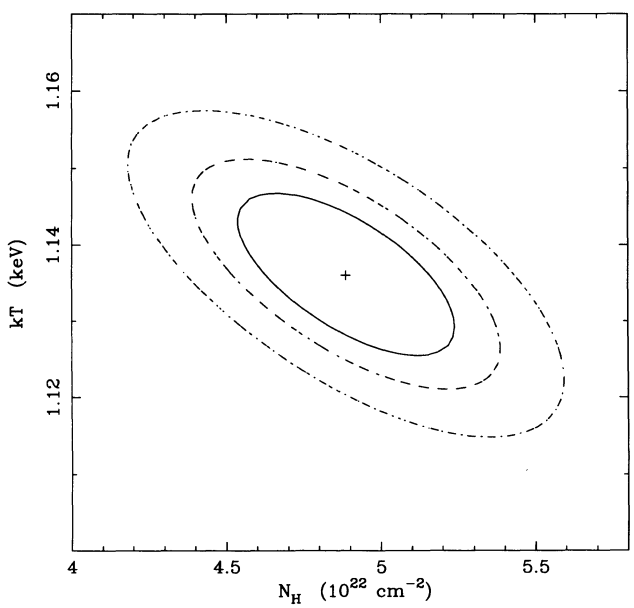

FIG. 4.—The χ^2 contours for the fitted values of the equivalent hydrogen column density and the blackbody temperature, derived from a two-dimensional grid. The contours represent changes in χ^2 of 2.30, 4.61, and 9.21, as appropriate for 1 σ, 90%, and 99% probability for two parameters of interest.

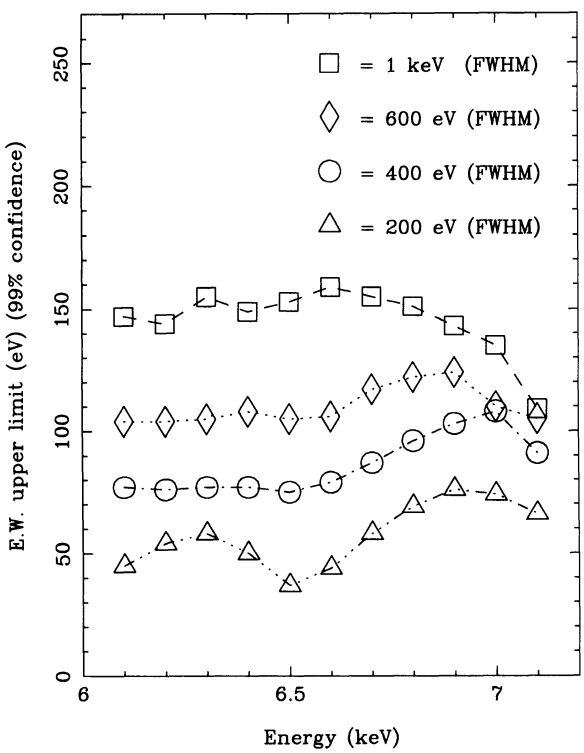

FIG. 5.—The upper limits on the presence of an iron line with a physical width 1 keV, 600 eV, 400 eV, and 200 eV. Upper limits are 99% confidence and are at a level far lower than previous iron line detections.

companion star (Milgrom 1976; Bonnet-Bidaud & van der Klis 1981). Molnar (1985) and Molnar & Mauche (1986) show that if the ADC model is extended to take into account the density stratification of the accretion disk bulge and the decrease of coronal intensity with height, the dependence of the modulation depth on energy is consistent with the ADC model, but hard to reconcile with the stellar wind and cocoon models.

From our best-fit parameters, we derive a radius for the blackbody emitting region of $R_{bb} = 30.9 \pm 3.0$ km (where the quoted error includes the uncertainties in the spectral fitting, the absolute flux calibration, and the ray-tracing required to model the vignetting). Such a radius is too large to be identified solely with the neutron star, and it seems likely that the inner disk regions contribute to the emission, perhaps as a consequence of an X-ray flare due to an increased mass accretion rate. Under these circumstances, the inner disk may become optically thick and expand azimuthally, shielding the outer disk and much of the corona from the bulk of the central X-ray flux. As the power-law and line emission components presumably arise in the outer disk area, corona, and/or heated face of the companion, this could explain the low level of these components in the BBXRT data.

Alternatively, it may be the case that the inner disk always produces a major blackbody component but that we normally see only a fraction of this emission due to the high inclination of the system. Then, the apparently high flux we observe with BBXRT may result from a decrease in the extent of the azimuthal disk structure that normally obscures much of the central emission. In this way, a *reduction* in the mass-accretion rate may lead to an *increase* in the level of direct flux observed. If the intensity of the line emission scales with the projected area of the bulge region, it would be correspondingly diminished.

REFERENCES

Becker, R. H., Robinson-Saba, J. L., Boldt, E. A., Holt, S. S., Pravdo, S. H., Serlemitsos, P. J., & Swank, J. H. 1978, ApJ, 224, L113
Blissett, R. J., Mason, K. O., & Culhane, J. L. 1981, MNRAS, 194, 77
Bonnet-Bidaud, J. M., & van der Klis, M. 1981, A&A, 101, 299
Chadwick, P. M., et al. 1985, Nature, 318, 642
Davidsen, A., & Ostriker, J. P. 1974, ApJ, 189, 331
Gregory, P. C., Kronberg, P. P., Seaquist, E. R., Hughes, V. A., Woodsworth, A., Viner, M. R., & Retallack, D. 1972, Nature, 239, 440
Harnden, F. R., et al. 1979, ApJ, 234, L51
Holt, S. S., Kaluzienski, L. J., Boldt, E. A., & Serlemitsos, P. J. 1979, ApJ, 233, 344
Kestenbaum, H. L., Ku, W. H.-M., Long, K. S., Silver, E. H., & Novick, R. 1978, ApJ, 226, 282
Kitamoto, S., Miyamoto, S., Matsui, W., & Inoue, H. 1987, PASJ, 39, 259
Kitamoto, S., Mizobuchi, S., Yamashita, K., & Nakamura, H. 1992, ApJ, 384, 263
Mason, K. O., Córdova, F. A., & White, N. E. 1986, ApJ, 309, 700
Mauche, C. W., & Gorenstein, P. 1986, ApJ, 302, 371
Milgrom, M. 1976, A&A, 51, 215
Molnar, L. A. 1985, Ph.D. thesis, Harvard University
Molnar, L. A., & Mauche, C. W. 1986, ApJ, 310, 343
Molnar, L. A., Reid, M. J., & Grindlay, J. E. 1988, ApJ, 331, 494
Nakamura, H., Matsuoka, M., Kawai, N., Yoshida, A., Miyoshi, S., Kitamoto, S., & Yamashita, K. 1993, MNRAS, 261, 353
Priedhorsky, W., & Terrell, J. 1986, ApJ, 301, 886
Pringle, J. E. 1974, Nature, 247, 21
Rajeev, M. R., Chitnis, V. R., Rao, A. R., & Singh, K. P. 1993, ApJ, in press
Serlemitsos, P. J., Boldt, E. A., Holt, S. S., Rothschild, R. E., & Saba, J. L. R. 1975, ApJ, 201, L9
Serlemitsos, P. J., et al. 1992, in Proc. 28th Yamada Conference of the Frontiers of X-ray Astronomy, ed. Y. Tanaka & K. Koyama (Tokyo: Universal Academy Press), 221
Smale, A. P., & Lochner, J. C. 1992, ApJ, 395, 582
Spencer, R., Swinney, R. W., Johnston, K. J., & Hjellming, R. M. 1986, ApJ, 309, 694
van der Klis, M., & Bonnet-Bidaud, J. M. 1989, A&A, 214, 203
van der Klis, M., & Jansen, F. A. 1985, Nature, 313, 768
van der Klis, M., Peacock, A., Smith, A., White, N., Mason, K., & Manzo, G. 1985, Space Science Rev., 40, 297
van Kerkwijk, M. H., et al. 1992, Nature, 355, 703
White, N. E., & Holt, S. S. 1982, ApJ, 257, 318